Summary of ATLAS Standard Model Results

Pierre-Hugues Beauchemin,[1] (on behalf of the ATLAS Collaboration)

[1]*Tufts University, 574 Boston Ave., Medford, Massachusetts, 02155, USA*

Abstract

Measurements of Standard Model (SM) processes at the LHC range from the production of jets and photons, or precision measurements with single W and Z bosons, to measurements of rare multiboson processes that recently became experimentally accessible. In this proceeding, recent measurements of such processes from the ATLAS collaboration are presented, with a focus on processes sensitive to Vector Boson Scattering. The results are used to determine fundamental parameters of the SM, such as the coupling constant of the strong interactions, constrain the parton content of the proton, or to set limits on non-SM electroweak gauge couplings. In all cases, the measurements are compared to state-of-the-art theoretical calculations.

Keywords: Vector Boson Scattering, Electroweak, QCD, Measurements, ATLAS,
DOI: 10.2018/LHEP000001

1. INTRODUCTION

The experimental studies of Standard Model (SM) processes and predictions constitute a crucial component of any High Energy Physics (HEP) endeavor aiming at understanding physics beyond the SM (BSM) in two different ways:

1. Precision measurements of SM properties constitute, de facto, model-independent searches for New Physics;
2. The sensitivity of any searches for BSM signal is fully limited by the precision, both experimental and theoretical, at which the SM contribution can be predicted in any data analysis aiming at discovering New Physics.

Let us consider the second impact first. Errors and uncertainties on SM predictions, i.e. on the background processes to be expected in any given searches for New Physics, can either lead to a false discovery claim, mask a potential discovery claim (in the case where the background predictions would be too large compared to what it should be), or simply alleviate the possibility to make a significant discovery claim (suppression of sensitivity due to too large uncertainties). To illustrate the first possibility, consider a BSM model that would have as main background a single Higgs produced via the gluon-fusion mechanism. As can be seen on Fig. 1 (taken from [1]), the SM predictions for this Higgs background process feature a 230% difference between the Leading Order (LO) and the Next-to-Leading-Order (NLO) prediction accuracies, with the theoretical uncertainty at LO being massively underestimated to be only about 15-20% of the LO prediction. Assuming that the experimental uncertainties are of the same order ($\approx$ 20%) and that the other backgrounds are negligible, such a discrepancy would entail that the observation of a data signal consistent with the NLO prediction would lead to a 7σ excess over a background estimated with the LO calculation, leading to a completely false discovery claim. Of course, one could argue that LO predictions cannot be taken seriously, but even a similar argument based on the NLO predictions compared to data consistent with the NNLO calculation would yield a 2.2σ excess, despite a quite large uncertainty on the NLO prediction. As shown on the figure, we would need to have the NNNLO calculation to really stabilize the robustness of discovery claims (or limits) that could be made in such a search. This is certainly not ubiquitous of all possible searches at the LHC, but clearly justifies the investment of resources and efforts in improving both SM-related theoretical calculations, as well as experimental uncertainties in SM-related measurements.

An example of payoff from such a coupled theoretical and experimental improvement in the precision of SM-related processes is offered by the most recent ATLAS Drell-Yan kinematic measurement [2]. The results reported constitute the first set of Z-boson double differential cross section measurements performed in the full phase-space of the decay leptons. They use approximate N^{4}LL resummation combined to approximate N^{3}LO fixed-order predictions to reach sub-percent level precision for a large range of Z-boson transverse momentum (p_T^Z) and rapidity (y^Z) values, as presented on the left panel of Fig. 2. The payoff of such unprecedentedly high precision can be seen on the right panel of Fig. 2, which presents the most precise strong coupling value ($\alpha_S(m_Z^2)$) measured at the scale of the Z-boson mass, as well as on the left panel of Fig. 3, which presents the very high sensitivity to PDFs this measurement offers. Because relative variations between $p_{T,W}$ and $p_{T,Z}$ at various rapidities are used to control the systematic uncertainties on the W-boson transverse-momentum spectrum and angular coefficients used in the W-mass measurement, such a precise Drell-Yan double differential cross section can be put to contribution for an improvement on the precision of m_W, a measurement that recently received a lot of attention because of the tension observed between the ATLAS and the CDF results, as presented on the right panel of Fig. 2. These examples convincingly illustrate how the field of HEP holistically profits from ever more precise SM measurements, testing state-of-the-art SM theoretical calculations, and offering evidences about where improvements are required, improvements that then feedback on the precision and accuracy of background predictions in searches for BSM signals.

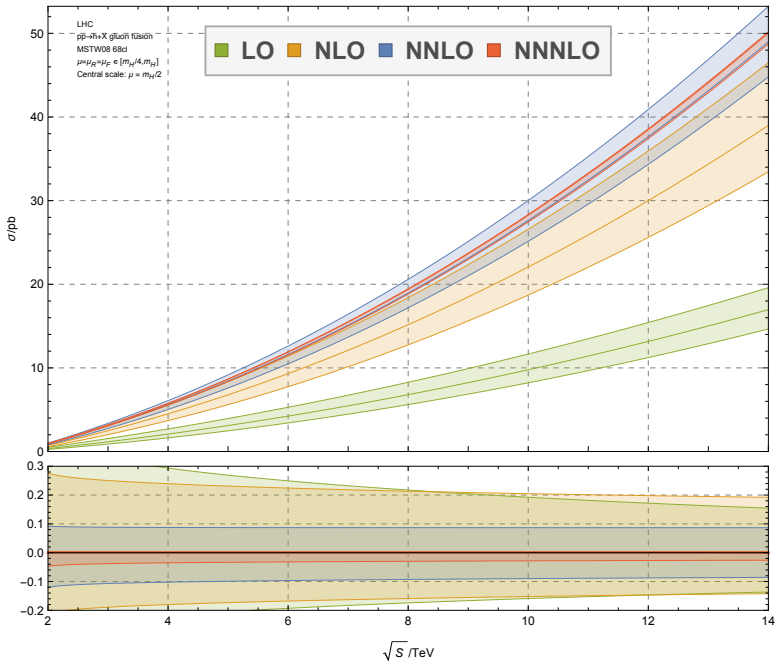

FIGURE 1: The Higgs gluon fusion cross section at all perturbative orders through N^{3}LO in the scale interval as a function of the center-of-mass energy $\sqrt{s}$ (taken from [1]).

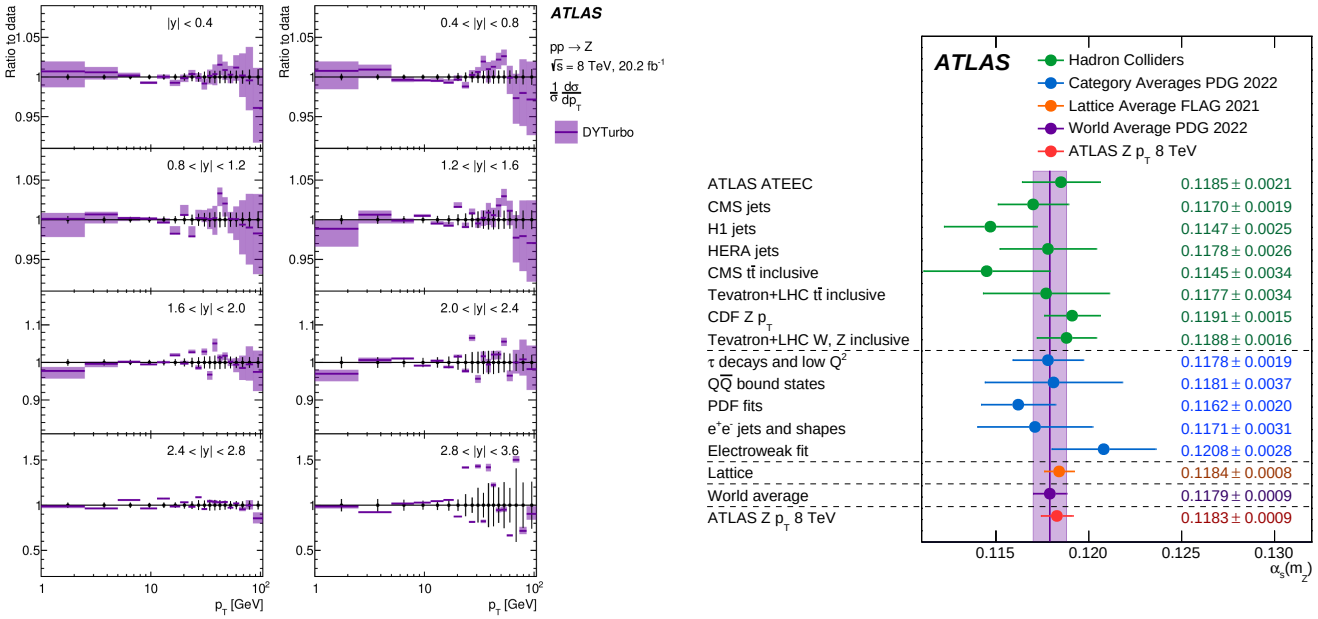

FIGURE 2: **Left:** Comparison between the measured absolute differential $\frac{d\sigma}{dp_T}$ cross sections in eight rapidity ($|y|$) bins, as published by ATLAS in [2], and the predictions from DYTurbo matched to the fixed-order $O(\alpha_S^3)$ contribution from MCFM [3, 4, 5]. Shown are the ratios between the predictions and the data. **Right:** Comparison of the determination of $\alpha_S(m_Z)$ from the Z-boson transverse-momentum distribution (ATLAS Z p_T 8 TeV) with other determinations. The figure is extracted from [6].

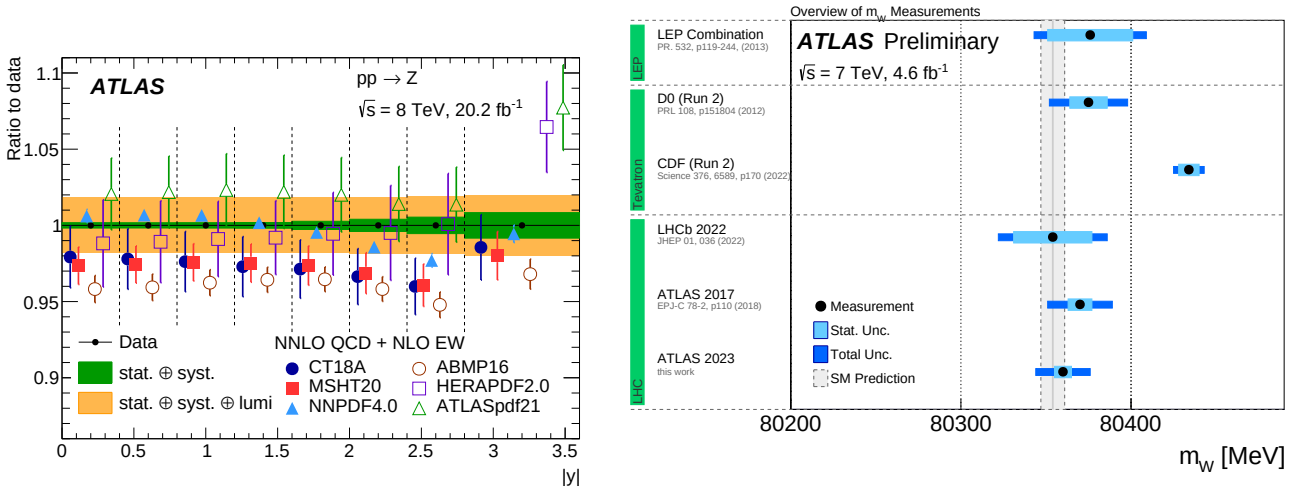

FIGURE 3: Left: Ratio comparison between the $\frac{d\sigma}{dy}$ ATLAS measurement ([6]) and NNLO QCD predictions obtained from DYTurbo using different NNLO PDF sets. The uncertainty bands in the predictions only show the uncertainties specific to each PDF set. **Right:** The most recent ATLAS measured value of m_W compared to the SM prediction from the global electroweak fit [7], and measurement results obtained at LEP, Tevatron, and other LHC analysis. The figure is obtained from [8].

The examples discussed up-to-now were related to deficiencies and improvements in pQCD predictions. Careful SM studies of the electroweak (EWK) interactions are however equally important for BSM physics, and provide an excellent set of illustrations of how SM measurements can directly be used to search for New Physics. For example, the precision measurements of the various EWK parameters of the SM, and their inclusion in global fits, can reveal severe inconsistencies pointing to issues with some measurements, or providing hints for New Physics in a way that does essentially not depend on assumptions about New Physics theories (model-independence). New precise measurements of the various SM EWK parameters would then provide more stringent consistency tests and could possibly resolve some of the observed tensions, but they could also lead to unresolvable discrepancies that would only be resolved in an extension of the SM. However, the SM measurements of rare processes, for which the cross section is at the level of a femtobarn, are of even more direct relevance to BSM considerations because they feature final states and kinematics that are typically very similar to those of many BSM signals of interest. Vector Boson Scattering (VBS) processes provide a particularly good example of such rare processes central to our understanding of the SM, while featuring high potential for a BSM discovery. From the SM perspective, VBS processes directly probe the electroweak symmetry breaking sector of the SM (the Higgs preventing the divergence of longitudinally polarized VBS amplitudes at high energy), providing a unitary test of the electroweak sector, while being sensitive to the non-abelian structure of the EWK interaction (gauge bosons self-couplings). These processes even allow for tests of pQCD because to be able to identify such an EWK VBS signal in a given final state that is statistically dominated by QCD-induced processes, an accurate modeling of pQCD is required, and so can be tested. From a BSM perspective, VBS events can be used to directly probe and constraint many BSM models because of their sensitivity to anomalous triple and quartic gauge couplings. An Effective Field Theory (EFT) approach can be used to parametrize any such BSM physics by the addition of higher-order dimension operators to the SM Lagrangian, without having to be more explicits about the details of the new interaction:

$$\mathcal{L}_{eff} = \mathcal{L}_{SM} + \Sigma_i \frac{f_i^{(6)}}{\Lambda^2}\mathcal{O}_i(6) + \Sigma_j \frac{f_j^{(8)}}{\Lambda^4}\mathcal{O}_j(8) \quad (1)$$

where i and j refer to the various kinds of operators of dimension (n) that can be conceived consistently with the basic symmetries assumed for the theory (e.g. Poincarre, SM gauge symmetries, etc.). The result of SM measurements could then be used to constraint the range of values the various dimensionless couplings $f_i^{(n)}$ can take, hence providing a set of generic limits to the class of all theories consistent with the dim-n operators being tested. For example, VBS SM measurement results are particularly useful to constrain the anomalous quartic gauge couplings (aQGCs) that appear, at lowest order in EFT, as Dim-8 operators of various Lorentz structures (scalar, tensor, mixed tensor-scalar, etc.), illustrating how SM measurements directly impact theoretical model-building activities.

The conjunction of all these various ways by which precision SM experimental investigations can impact New Physics searches clearly explain why, despite how complicated and resource-demanding these SM data analyses are, they constitute a very large and important component of the physics programs of LHC experiments, and why they should retain the attention of the theoretical BSM community. This proceeding will present in more details both the SM and the BSM information that can be extracted from three specific VBS SM measurements recently completed by the ATLAS Collaboration with Run-2 $\sqrt{s}$ =13 TeV data.

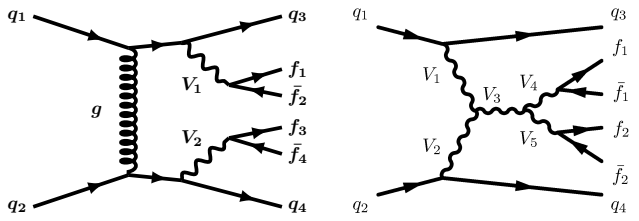

FIGURE 4: Representative Feynman diagrams for a $VVjj$ ($V = W/Z/\gamma$) production with a scattering topology that is suppressed by a same-sign dilepton final-state selection.

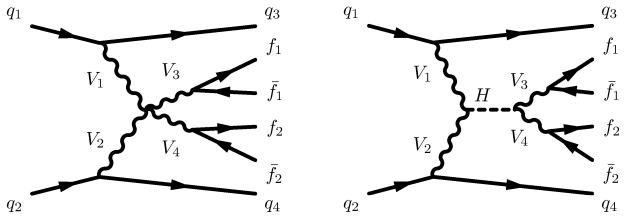

FIGURE 5: Representative Feynman diagrams for a $VVjj$ production with a scattering topology that is not suppressed by a same-sign dilepton final-state selection either in the SM (diagram on the left) or in some BSM extensions (diagram on the right, when, for example, the scaler propagator in the diagram represents a doubly charged Higgs).

2. ATLAS VECTOR BOSON SCATTERING MEASUREMENTS

2.1. Same Sign W pair plus 2-jets ($W^{\pm}W^{\pm}jj$)

The first set of measurements to be discussed consists in a detailed study of same-sign W-pair plus two jets events[1]. The $W^{\pm}W^{\pm}jj$ final states are ideal for studying VBS signals because they feature the largest EWK-to-QCD production cross section ratio compared to other VBS diboson processes, while suffering from little SM background. The main reason behind this is that the same-sign lepton selection more largely suppresses non-VBS than VBS contributions to the diboson production final states, and eliminates most of the dilepton SM signal background events, which are typically produced with opposite-sign leptons (Drell-Yan, top pair production, etc.). This is illustrated in Fig. 4: diboson production processes involving strong interaction vertices (as illustrated by the Feynman diagram on the left), as well as electroweak-only VBS scatterings in an s-channel (as illustrated by the diagram on the right), will only feature opposite-sign W-boson pairs in the final state due to electric charge conservation, which will largely be suppressed by the selection of same-sign charged leptons in the final state. This does however not apply to SM VBS processes involving a quartic gauge coupling (as presented for example on the left of Fig. 5), which constitute the signal of interest. The selection of events with charged leptons of same sign is therefore a very powerful way to select VBS events, in addition of enhancing the QGC signal. Note however that the Feynman diagram on the right of Fig. 5, while also being suppressed in the SM by the same-sign selection, would not suffer from such a selection in many BSM models in which, for example, the Higgs in the propagator of the VBS s-channel depicted on this Feynman diagram is replaced by a doubly-charged Higgs from theories with an extended Higgs sector. The sensitivity to such a non-SM contribution and to anomalous quartic gauge couplings (aQGC) make the search for New Physics in this final state particularly promising for a discovery.

In addition of requiring two same-sign charged leptons in the final state, the VBS signal is enhanced by requiring a rapidity gap between the two hardest jets in the event ($|\Delta y(jj)| > 2.0$) with an invariant mass of at least 500 GeV ($m_{jj} > 500$ GeV). In this kinematic region, the EWK contribution to the $WWjj$ production amount to 52% of all events, with only a 5.4% of the events coming from $WWjj$ Feynman diagrams involving at least one strong coupling vertex (with a QCD-EWK interference contribution of less than 2%). The rest of the events mostly consist of WZ and non-prompt lepton backgrounds. After background subtraction, efficiency correction, and unfolding of the detector effects, the measurement of the EWK contribution to $W^{\pm}W^{\pm}jj$ resulted in a cross section of $\sigma = 2.92 \pm 0.22(\text{stat.}) \pm 0.19(\text{syst.})$fb. This cross section was obtained from a likelihood fit to four independent measurements of the cross section in the ee, $e\mu$, μe and $\mu\mu$ channels. Predictions obtained at LO accuracy ($\alpha^4_{ewk}\alpha^2_S$ for the QCD production, α^6_{ewk} for the pure EWK contributions, and $\alpha^5_{ewk}\alpha^1_S$ for their interferences) from the MagGraph5_AMCNLO generator interfaced to Herwig7 for the parton shower, including some partial NLO pQCD corrections derived from Sherpa 2.2.11, yielded a total EWK $W^{\pm}W^{\pm}jj$ cross section of $\sigma = 2.53 \pm 0.04(\text{PDF}) \pm^{0.22}_{0.19}(\text{scale})$fb, with the systematic uncertainties stemming from the choice of PDF, renormalization scale, and factorization scale. This corresponds to about a 1σ excess of data over the prediction. Measuring differential cross sections and comparing them to other predictions provide further insight on the origin of such a tension between data and predictions. The measurement results for some of such differential cross sections are presented in Fig. 6. We can see in this figure that while the small excess of data over predictions is not much dependent on the accuracy of the description

[1] A detailed report of these results is presented in [11]

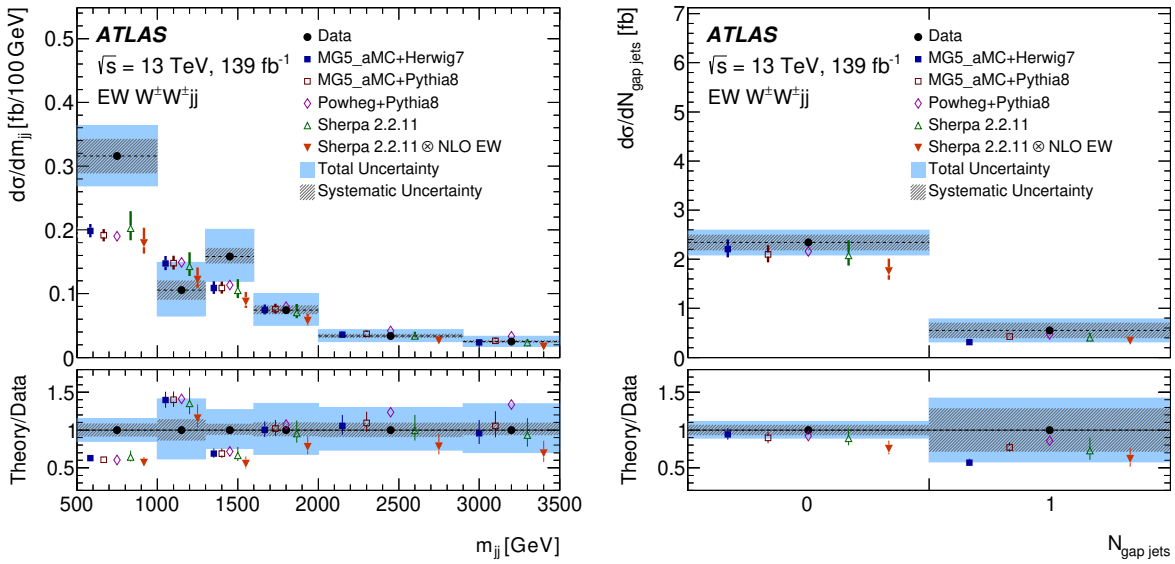

FIGURE 6: Fiducial differential cross sections for the EWK $W^{\pm}W^{\pm}jj$ production as a function of: **Left:** the invariant mass of the two leading jets in the event (m_{jj}); **Right:** The number of jets measured in the rapidity gap between the two leading jets in the event.

of the radiation of a third jet in the rapidity gap between the two leading jets in each event (right panel), the invariant mass of the two leading jets (left panel) is poorly modeled in the 500GeV $< m_{jj} <$ 1.5TeV region by all the different predictions.

Despite some issues in the modeling of SM VBS processes by current generators, the predictions remain in reasonable agreement with the data, and no significant excess is observed. These data can therefore be used to calculate limits on BSM models to which the measurement is sensitive. To this end, the unfolded measurement result for the total (EWK+QCD+Interference) $W^{\pm}W^{\pm}jj$ differential cross section as a function of the invariant mass of the two charged leptons ($m_{\ell\ell}$), as presented on the left panel of Fig. 7, is used as a starting point. Equation 1 is then used to calculate the BSM predictions for a set of nine independent charge-conjugate and parity-conserving D-8 effective operators relevant to the WWWW quartic gauge couplings (the coefficients of the dim-6 operators are assumed to all be zero). Matrix elements are calculated at LO accuracy for each operator, and MC samples are generated with MadGraph5_AMCNLO 2.65, interfaced to Pythia8.235, for each terms separately ((SM, interference, quadratic), setting the coefficient $c_i = \frac{f_i^{(8)}}{\Lambda^4}$ to 1 for each case. Each sample is then multiplied by its appropriate signal strength parametrized by c_i, $|c_i|^2$, or $c_i c_j$. A likelihood function is calculated using a Poisson distribution with systematic uncertainties implemented via Gaussian constraints. For each individual coefficient c_i (setting all other coefficients to zero), as well as for each non-zero pair c_i, c_j (for two-dimensional limits), maximum likelihood fits are performed, maximizing the likelihood with respect to the nuisance parameters. Confidence intervals are derived assuming that the profile likelihood test statistic is χ^2-distributed.

While EFT provides a very powerful framework for constraining classes of models in a generic way from model-independent measurement results, suppressing biases one could have toward a particular model, and providing the input for testing models that have even not yet been conceived, it suffers from one drawback: it relies on the scale Λ to be much larger than the kinematic scales probed with the measurement. For TeV-value Λ scales, this assumption breaks at the LHC, limiting the validity of the constraints calculated with an EFT framework, and even violating unitarity at tree-level in some corners of the probed phase space. To quantify how important this effect is, limits are obtained by removing any BSM contribution to the $W^{\pm}W^{\pm}jj$ predictions in phase space volumes with kinematic large enough to threaten unitarity. Such phase space is selected from restriction on the maximum invariant mass of the diboson system at parton level (m_{WV}) in which New Physics is included (cut-off scale). The smaller is the cut-off on m_{WV}, the smaller will be the phase space in which New Physics will be added to the SM predictions, and the larger will be the SM contribution for a given value of Λ. We therefore expect to exclude a smaller range of c_i values for smaller cut-off scales. This is illustrated on the middle panel of Fig. 7 obtained for one of the tensor operators ($\mathcal{O}_{T1}$) predicting a BSM contribution to the $W^{\pm}W^{\pm}jj$ final states. We can see the values of $c_{T1} = \frac{f_{T1}^{(8)}}{\Lambda^4}$ excluded at 95% CL when the actual SM measurement results are used to calculate the limit (black full line), as well as when only the SM expectations are used in the limit calculation (dash blue line). This plot also presents, in green, the unitarity limit, i.e. a theory-based constraint on the values of c_{T1} resulting from excluding any event in the phase space selected with the m_{WV} restriction for which the kinematic exceeds Λ. We can see that up to about 2.5 TeV, the experimental limits are more constraining than the theoretical limits, but above this scale, requiring the predictions to satisfy unitary is more constraining on the c_{T1} parameter than the data are. It is not all the parameters that feature similar constraints from theory and data. For example, the right panel of Fig. 7 presents the limits for the c_{M0} parameter controlling the contribution of effective operators built from two Higgs boson covariant derivatives and two field-strength tensors to the $W^{\pm}W^{\pm}jj$ predictions. We can see that the unitarity limits are more constraining than the experimentally observed limits for all the cut-off scales above

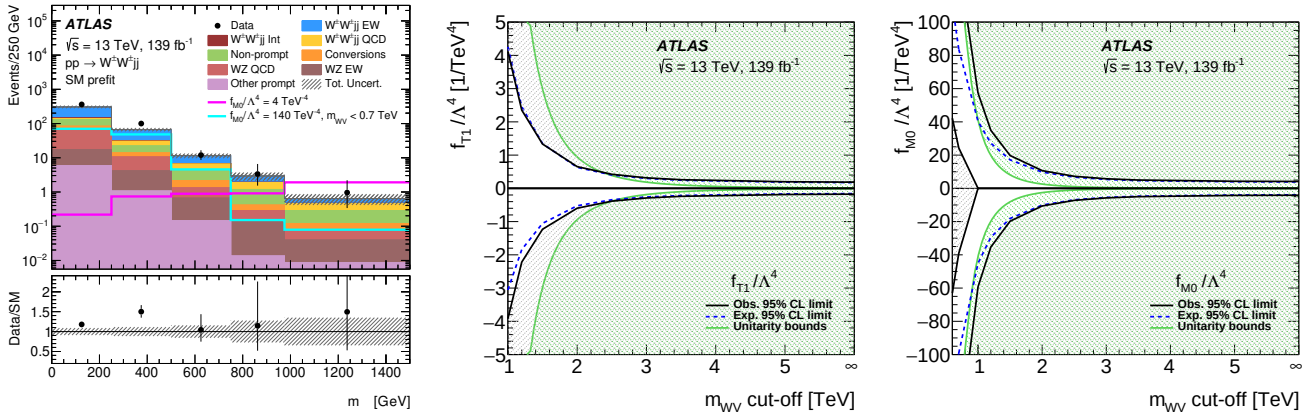

FIGURE 7: Left: The observed $m_{\ell\ell}$ distribution and the SM expectation. The hatched error band corresponds to the total uncertainty. The impact of BSM contributions is illustrated with two examples obtained with the EFT framework. **Middle:** Evolution of the one-dimensional expected (blue dashed line) and observed (black line) limits at 95% CL on the parameter corresponding to the quartic operators $\mathcal{O}_{T1}$ as a function of the cut-off scale m_{WV}. The green line corresponds to the unitarity limits as a function of the same cut-off scale. The filled area corresponds to parameter values excluded either by the data at 95% CL or by the unitarity condition imposed on the theory. **Right:** Same as the middle plot but for the parameter corresponding to the quartic operators $\mathcal{O}_{M0}$.

800 GeV. Surprisingly, this exclusion plot also tells us that a null value of the c_{M0} parameter is excluded at 95% CL by the data for low m_{WV} cut-off scales. This is explained by the shape of the EFT prediction for the $\mathcal{O}_{M0}$ operator, which exhibits a peak at $m_{\ell\ell}$ values around 400 GeV, where an upward fluctuation is also present in data, as seen on the left panel of Fig 7, leading to a double-minimum shape for the test statistic.

If we assume that two of these BSM effective operators can both contribute to the $W^{\pm}W^{\pm}jj$ final states used in the VBS measurements, the limits on these two effective operators will be stronger than what was shown for the 1-dimensional limits in Fig. 7. We can for example see on the left panel of Fig. 8 the exclusion plane for the c_{M0} and the c_{M1} parameters, assuming a unitarisation cut-off scale of 1.5 TeV. The coefficient values outside the circles are excluded at 95% CL. In this example, the predicted differential yields of the two operators are anti-correlated, explaining why the weakest excluded values for each operator are reached when their coefficients have the same sign. The figure also shows how the expected limits would change if the expected yield would be varied by one (green) or two (yellow) standard deviations. The two-dimensional unitarity bounds are represented on the plot by the two parallel green lines. As can been seen, theoretical and experimental exclusions complement each other because some regions of the parameter space are excluded by one but not the other, and vice versa. This observation applies to most of the Dim-8 EFT parameters sensitive to this $W^{\pm}W^{\pm}jj$ measurement, with the notable exception of the $\mathcal{O}_{S02}$ vs $\mathcal{O}_{S1}$ operators that are almost 100% correlated, and for which the unitarity limits are systematically tighter than the experimental ones, as presented on the middle panel of Fig. 8.

It is finally interesting to note that such a SM VBS-oriented measurement can also be used to test quite specific BSM models of interest. For example, the results from this measurement can be interpreted in terms of a search for a doubly-charged Higgs boson produced in VBF processes and further decaying into two same-sign W bosons. Such a process can for example happen in BSM models featuring an extended Higgs sector with additional isotriplet scalar fields, like in the Georgi and Machacek (GM) model [9]. The right panel of Fig. 8 presents the limits on the production cross section times branching ratio for a fermiophobic doubly charged Higgs ($H_5^{\pm\pm}$) decaying to a pair of same-sign W-bosons, as a function of the mass of this doubly-charged Higgs, assuming the GM model. Note that there is a local excess of events over the SM prediction in the measured invariant mass distribution at around 450 GeV, which explains the difference observed between the expected and observed limits around $m_{H_5^{\pm\pm}} = 500$ GeV. The global significance of this excess is 2.5 standard deviations.

From all these results, we can see better how and why SM measurements of VBS processes provide an ideal gateway to BSM physics, while providing essential elements for a better understanding of the SM physics. The $W^{\pm}W^{\pm}jj$ final states are however not the only ones to offer such opportunity, and below we consider other examples thoroughly studied with Run-2 ATLAS data.

2.2. *Four Charged Leptons in Association with 2 Jets ($Z(\to \ell\ell)Z(\to \ell'\ell')jj$)*

The pair-production of Z-bosons in association with two jets, where the two Z-bosons decay to charged leptons, constitute a set of processes complementary to the $W^{\pm}W^{\pm}jj$ production in enabling thorough studies of Vector Boson Scattering[2]. Similarly to what was presented in the previous section, the $Z(\to \ell\ell)Z(\to \ell'\ell')jj$ final states can be produced via processes involving only EWK vertices, including diagrams sensitive to the WWZ triple gauge coupling (e.g. the $V_1V_2V_3$ vertex on the right panel of Fig. 4) or to the WWZZ weak-boson self-interactions (left panel of Fig. 5), both arising from the non-Abelian nature of the electroweak interaction.

[2] A detailed report of these results is presented in [12]

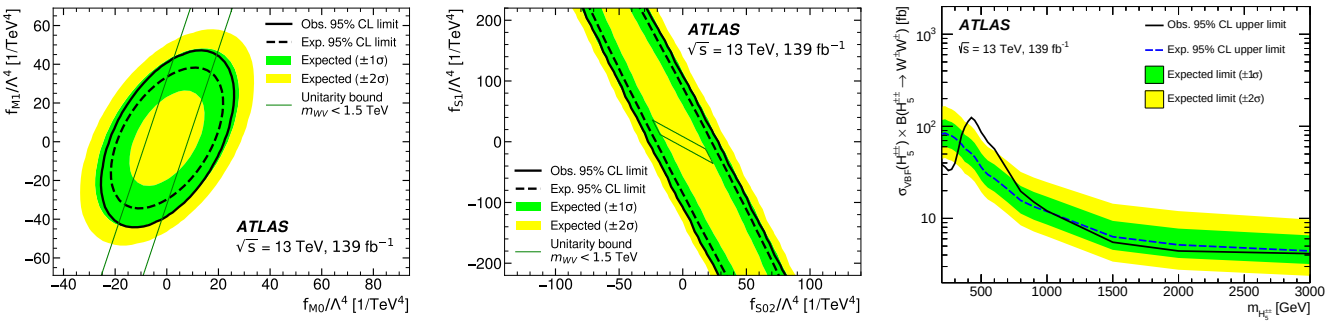

FIGURE 8: Left: Two-dimensional median expected (dashed line) and observed (solid line) 95% CL intervals on parameters corresponding to the M0-M1 EFT quartic operator combination, with a unitarisation cut-off scale of 1.5 TeV and unitarity bounds (green line). The one (green) and two (yellow) sigma bands show the 68% and 95% CL regions for the expected limit curves, respectively. **Middle:** Same as the left plot but for the parameters of the S1-SO2 EFT operators. **Right:** Expected and observed exclusion limits at 95% CL for $\sigma_{\mathrm{VBF}}(H_5^{\pm\pm}) \times B(H_5^{\pm\pm} \to W^{\pm}W^{\pm})$ as a function of $m_{H_5^{\pm\pm}}$. The green (yellow) band is the 68% (95%) confidence interval around the median expected limits.

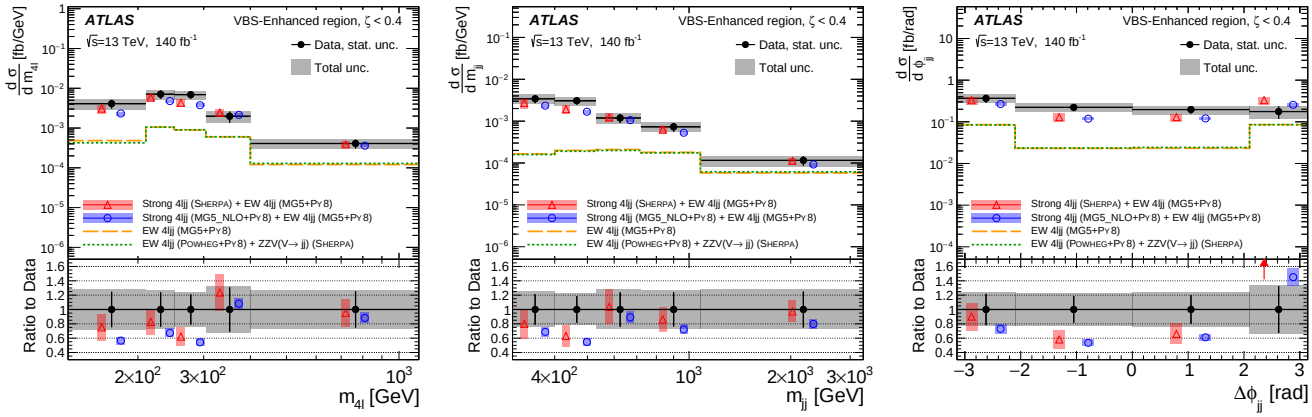

FIGURE 9: Differential cross sections for inclusive $4\ell jj$ production in the VBS-enhanced region as a function of $m_{4\ell}$ (**Left**), m_{jj} (**Middle**), and $\Delta\phi_{jj}$ (**Right**). The data are represented as black points and the associated error bars represent the statistical uncertainty. The total uncertainty in the measurement is represented as a grey hatched band. The data are compared with two theoretical predictions, estimated by using Sherpa (triangles) and MadGraph5 (circles) for the strong $4\ell jj$ contribution and MadGraph5 for the EWK $4\ell jj$ contribution. The band on the theoretical predictions represents the theoretical uncertainty. The dashed lines show the contribution of EWK contribution to the differential cross sections as predicted by MadGraph5lo and POWHEG+Pythia8, with the s-channel contributions from the ZZV production obtained from Sherpa.

The two final-state jets at tree-level can also arise from the strong interaction, with the final state quarks each emitting a Z-boson, as illustrated on the left panel of Fig. 4). Because both Z-bosons decay to opposite-sign charged leptons, it is not possible to suppress the strong interaction contribution like in the $W^{\pm}W^{\pm}jj$ case. This has nevertheless the virtue of rendering the measurements of ZZjj production rate and kinematic properties very sensitive to the strong interaction, allowing for testing the accuracy of the state-of-the-art pQCD calculations. The Vector Boson Scattering contribution can nevertheless be enhanced over the QCD contribution by requiring that the invariant mass of the two jets is large ($m_{jj} > 300$ GeV), that there is a rapidity gap between these two jets ($|\Delta y_{jj} > 2.0$), and that the centrality of the four-lepton system, defined as $\zeta = |\frac{y_{4\ell} - 0.5(y_{j_1} + y_{j_2})}{\Delta y_{jj}}|$, where $y_{4\ell}$ is the rapidity of the four-lepton system and y_{j_i} the rapidity of the jet i ($i = 1, 2$), is high ($\zeta < 0.4$). With these selections, the ratio of QCD-to-EWK contribution to the ZZjj processes is 4-to-1, while it is about 20-to-1 if the centrality selection is reversed ($\zeta > 0.4$).

Once again, selected data samples are corrected for background, efficiencies, and detector effects (unfolding), with a comprehensive set of systematic uncertainties estimated for each of these corrections. The differential cross section measurement results thus obtained are compared to state-of-the-art theoretical predictions obtained at LO accuracy from MadGraph5+Pythia8 for the EWK $4\ell jj$ processes and either Sherpa 2.2.2 (NLO accuracy for the first parton emission, LO for the following three emissions) or MadGraph5_aMCNLO+Pythia8 (NLO on the first parton emission only) for the strong $4\ell jj$ processes.

As can be seen on Fig. 9, the prediction obtained using Sherpa for the strong production is found to be in satisfactory agreement with the data for all measured distributions in the VBS-enhanced region (red triangles on the figure). However, the prediction obtained using MadGraph5+Pythia8 for the strong production is found to underestimate the inclusive cross section in all distribu-

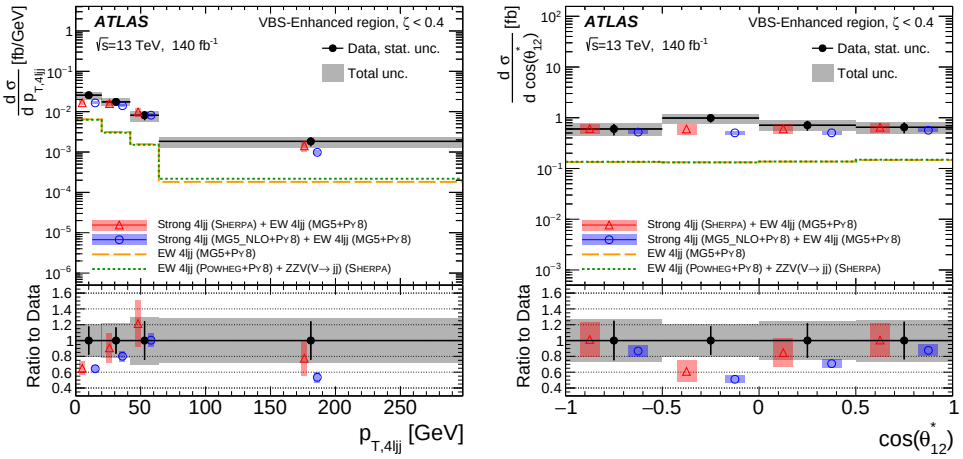

FIGURE 10: Differential cross sections for inclusive $4\ell jj$ production in the VBS-enhanced region as a function of $p_{T,4\ell jj}$ (**Left**) and $\cos\theta^*_{12}$ (**Right**). The predictions and the uncertainties are constructed as explained in Fig. 9.

tions, with a disagreement especially noticeable at low m_{jj}, low $m_{4\ell}$, and low $|\Delta\phi_{jj}|$. The plots on the figure also present the pure EWK contribution as calculated by default with MadGraph5+Pythia8 (dashed green line), but also with an alternate calculation using contributions from both POWHEG+Pythia8 and Sherpa 2.2.2. These calculations do however not feature any differences for the distributions measured in this analysis. We can see that as m_{jj} and $m_{4\ell}$ increase, the fraction of ZZjj events coming from the EWK process largely increases, rendering these two observables particularly sensitive to the VBS component of the ZZjj production. The fact that the data agree well with the prediction in the tail of these distributions means that this EWK contribution is well-modeled by the predictions, and it is the QCD part of the MadGraph5+Pythia8 calculation which is the cause of the observed discrepancies. This can be explained by the fact that MadGraph5+Pythia8 relies on the Pythia8 parton shower to model the 3rd jet in the event, while Sherpa models it with a matrix element at LO accuracy. Since the event selection identifies the two 'tagging' jets as the highest transverse momentum jets that satisfy $\eta_1 \times \eta_2 < 0$, the third-highest transverse momentum jet in the event will be selected in some instances. This jet is better described in Sherpa than in MadGraph5+Pythia8. The mismodeling of extra radiation is even more striking in the measurement of the recoil of the $4\ell jj$ system ($p_{T,4\ell jj}$) presented on the left panel of Fig. 10, a quantity essentially insensitive to the EWK contribution to the ZZjj processes. These measurements indicate the need for higher-order pQCD predictions for a better accuracy in the SM description of the ZZjj events at the LHC. Note that the EWK interest in such measurements is not limited to the VBS production mechanism for ZZjj final states. For example, the $|\Delta\phi_{jj}|$ variable is particularly sensitive to the charge conjugation and parity structure of the WWZ and the WWZZ interactions. Similarly, the polarization of the Z-boson can be probed using the cosine of the angle between the negatively-charged lepton and the Z-boson as measured in the centre-of-mass frame of the Z-boson ($\cos\theta^*$). The right panel of Fig. 10 presents the measurement of the cosine angle sensitive to the polarization of the leading Z-boson candidates.

Similarly as in the case of the $W^\pm W^\pm jj$ analysis, the results of the ZZjj $m_{4\ell}$ and m_{jj} measurements just presented, featuring no significant deviation with respect to the predictions, and therefore not providing any hint for New Physics, can be used to constrain, in a model-independent way, BSM models. The strategy, again, is to use an EFT framework to set limits on the parameter values of Dim-8 effective operators. 95% confidence intervals on nine of these effective operator coefficients are obtained, with the two most tightly constrained coefficients presented in Fig. 11. Once again, the limits are obtained as a function of a cut-off scale E_c defined as $m_{4\ell} < E_c$, preventing important unitarity violation at large energy scales. Both of the constrained coefficients presented in Fig. 11 feature tighter experimental constraints for cut-off scales of about 1 TeV, but tighter theoretical constraints (unitarity bounds), for larger cut-off scales. In all cases, all the tested effective operator coefficients are consistent with zero.

2.3. Polarization and CP-properties in $Z(\to \ell\ell)Z(\to \ell'\ell')$ Events

This experimental study constitutes a set of dedicated measurements that significantly improve the sensitivity to polarization and CP-properties of the Z-boson over what was achieved by the $ZZjj$ measurements reported above[3]. The focus on longitudinal polarization of massive weak boson is a direct probe of the Electroweak Symmetry Breaking mechanism, through which the W- and Z-bosons obtain their longitudinally polarized states, and provide a unique sensitivity to BSM physics, especially to those models featuring an anomalous neutral triple gauge coupling (aNTGC). In addition, the measurement of CP-sensitive observables in diboson production can be utilized to study the violation of CP-symmetries required to explain the matter-antimatter asymmetry in the universe, known to be insufficient in the SM. The goal is to explore new sources of CP-violation in the gauge-boson sector using the EFT framework with operators sensitive to aNTGC vertices, their contribution to the ZZ processes being parameterized by the two dimensionless couplings f_Z^4 and f_γ^4. To this end, this analysis focuses on the differential cross section measurement

[3] A detailed report of these results is presented in [13]

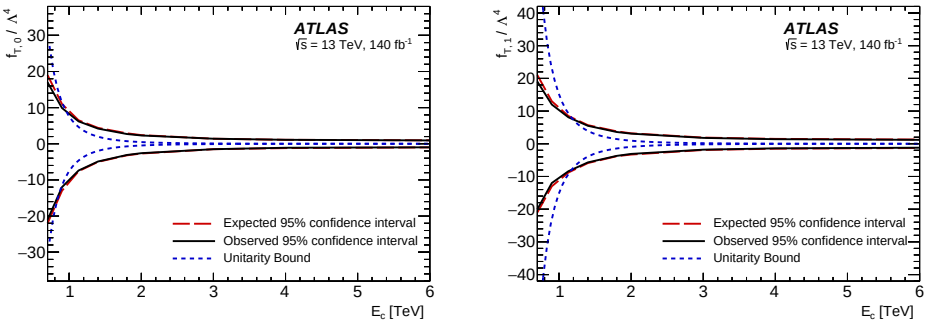

FIGURE 11: Expected and observed 95% confidence interval for the $f_{T,0}$ (**Left**) and $f_{T,1}$ (**Right**) effective operator coefficients as a function of a cut-off scale, E_c, which restricts the interference- and pure dimension-eight- contributions to have $m_{4\ell} < E_c$. The constraints are obtained using a two-dimensional fit to the $4\ell jj$ differential cross sections measured as a function of $m_{4\ell}$ and m_{jj}.

of a dedicated CP-odd angular observable, referred to as the Optimal Observable ($\mathcal{OO}$), defined from the $\ell\ell\ell'\ell'$ (where ℓ is a muon or an electron) decay products of longitudinally polarized Z-bosons in diboson production (Z_LZ_L). The comparison of the measurement results with state-of-the-art predictions is then used to constrain CP-violating effective operators especially sensitive to the interference between SM and BSM terms of the EFT theory.

In this analysis, a Boosted Decision Tree (BDT) algorithm, based on angular variables, is used to separate Z_LZ_L states from either fully transverse or mixed polarization diboson states. The Z_LZ_L fraction is obtained from a binned maximum likelihood fit to the BDT distribution using a different template (generated at LO with MadGraph5+Pythia8, but reweighted using a sophisticated combination of NLO calculations) for each polarization state, as well as for the background, as illustrated on the left panel of Fig. 12. The result of the fit yields a fiducial cross section for the Z_LZ_L production of $\sigma^{obs}_{Z_LZ_L} = 2.45 \pm 0.56(\text{stat.}) \pm 0.21(\text{syst.})\text{fb} = 2.45 \pm 0.60\text{fb}$, consistent with the SM prediction of $\sigma^{pred}_{Z_LZ_L} = 2.10 \pm 0.09\text{fb}$. For the differential cross section measurement of the Optimal Observable, first an angular observable is formed from the CP-sensitive azimuthal angles ϕ_1 and ϕ_3, giving a direct measure of the Z-boson spin when reconstructed in the reference frame illustrated on the middle panel of in Fig. 12, and from the CP-sensitive polar angles θ_1 and θ_3 between the negatively charged final-state lepton in the Z_1 (Z_2) rest frame and the direction of flight of the Z_1 (Z_2) boson in the four-lepton rest frame, as also illustrated on the figure. This angular observable is defined as: $T_{yz,1(3)} = \sin(\phi_{1(3)}) \times \cos(\theta_{1(3)})$. It maximizes the asymmetry for each Z-boson system. Starting from the 2D distribution of $T_{yz,3}$ vs $T_{yz,1}$, the $\mathcal{OO}$ observable $\mathcal{O}_{T_{yz,1}T_{yz,3}}$ is formed as a 2D-to-1D mapping grouping together sensitive and non-sensitive bins of T_{yz} to improve the sensitivity to CP-odd BSM couplings in the four-lepton final states. The unfolded differential cross section measurement result on the $ZZ \to 4\ell$ production as a function of $\mathcal{O}_{T_{yz,1}T_{yz,3}}$ is presented on the right panel of Fig. 12 and is compared with two different SM predictions, one obtained with the Sherpa generator and the other obtaiined with POWHEG. For each bin, the measured cross section on the data agrees closely with both sets of predicted cross sections. With such an absence of significant discrepancy between data and SM expectations, 95% confidence level exclusion limits are set on two different CP-odd aNTGC parameters (f^4_Z and f^4_γ) using only the linear interference terms between SM and BSM in the EFT (i.e. that the quadratic contributions are set to zero). A comparison to the limits when the quadratic terms are included is also provided. Results are presented in the Table 1 below. Adding the quadratic terms improves the limits by one order of magnitude, but this is still not enough to be competitive with limits obtained from simple diboson events (see for example [10]), because the $\mathcal{O}_{T_{yz,1}T_{yz,3}}$ observable, while much more sensitive to CP states, is not sensitive to the high-p_T regime, more important for BSM discoveries.

	Interference Only		Full	
a NTGC Parameter	Expected	Observed	Expected	Observed
f^4_Z	[-0.16,0.16]	[0.12,0.20]	[-0.013,0.012]	[-0.012,0.012]
f^4_γ	[-0.30,0.30]	[-0.34,0.28]	[-0.015,0.015]	[-0.015,0.015]

TABLE 1: Limits on two aNTGC operators using the $\mathcal{O}_{T_{yz,1}T_{yz,3}}$ measurement result.

3. CONCLUSION

QCD and EWK processes are together pervasive of all particle physics phenomena to be studied at the LHC. A large portion of the physics program of the various LHC experiments is dedicated to measurements allowing to improve our modeling of QCD and EWK effects in the phase spaces probed with the data the select. These measurements aim at high precision and are therefore technically and conceptually challenging. Overcoming these challenges is however essential to maximize the physics messages the LHC experiments deliver to the broader experimental and theoretical HEP communities. In this document, we presented a summary of

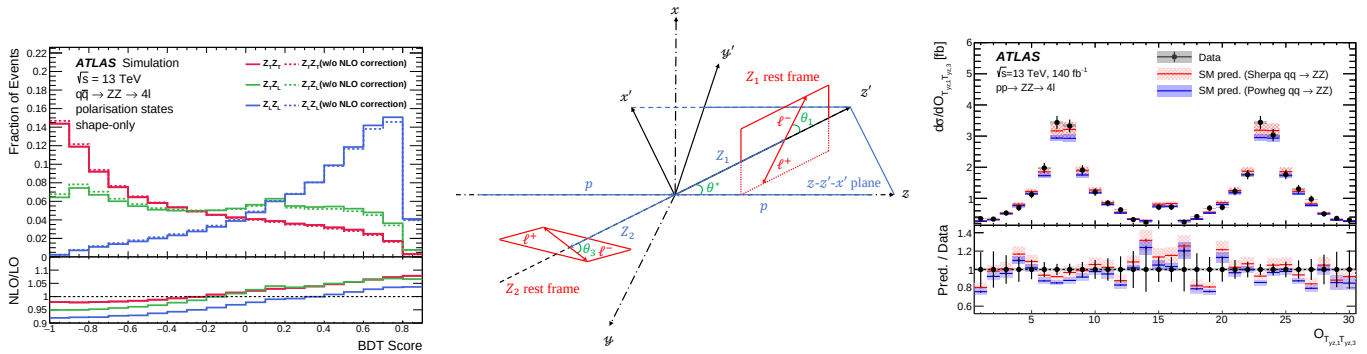

FIGURE 12: **Left:** BDT distributions of the three polarization templates for the $q\bar{q} \to ZZ$ process, before (dashed lines) and after (solid lines) using a reweighting procedure to account for higher-order pQCD corrections. All distributions are normalized to the same area. The lower panel shows the ratio of the templates after the corrections to those before the corrections. **Middle:** Definition of the angles used in the polarization measurement as well as the reference frame used to define the CP-sensitive angles. The xyz-frame (dot-dashed) is the laboratory frame with the z-axis along the beam direction. The x′y′z′-frame (solid) is a new frame used to define the CP-sensitive angles. The z′-axis is defined as the direction of motion of the Z_1 boson in the four-lepton rest frame. The x′-axis defines the reaction plane containing the laboratory z-axis and the z′-axis. The right-hand rule gives the y′-axis. **Right:** Unfolded differential cross section as a function of the Optimal Observable $\mathcal{O}_{T_{yz,1}T_{yz,3}}$. The grey, red and blue uncertainty bands represent the respective systematic uncertainties in the measured unfolded cross section and predicted particle-level cross sections, where the $q\bar{q} \to ZZ$ contribution is predicted using either the Sherpa or POWHEG generators. The vertical error bars represent the total uncertainties in the measured differential cross section.

a very small sample of such measurements. We presented the results of a double differential cross section for Drell-Yan and showed how state-of-the-art calculations at approximate N^{4}LL matched to approximate N^{3}LO accuracy allowed to yield best measurement results, feeding back into precision measurements of SM parameters such as α_S, for example. This proceeding however focused on a presentation of the most recent measurement results for diboson processes sensitive to Vector Boson Scattering. First we considered same-sign WW plus 2 jets events with selections enhanced for the VBS contribution. From the differential cross section measurements that were presented, we concluded that the EWK contribution to the observables measured in the $W^{\pm}W^{\pm}jj$ final states was well modeled by theoretical predictions, even if these predictions are only calculated at LO accuracy. Such conclusion did however not apply to the QCD contribution, especially for the measured observables sensitive to the modeling of a third jet in each event. The exact same conclusions were obtained from the results of similar measurements in $Z(\to \ell\ell)Z(\to \ell'\ell')jj$ events. These results therefore provide crucial information to the theory community about how diboson predictions could be improved in phase space volumes with potentials for New Physics discoveries. The good accuracy of the description of EWK phenomena was further confirmed by dedicated measurements of the longitudinal polarization and of CP-states in ZZ events.

Despite some tensions between the data and the predictions in the results obtained due to QCD modeling effects, the agreement was good enough to conclude that there is no evidence for New Physics in these data, so the measurement results could be used to constraint BSM models. A generic approach was adopted using an EFT framework where limits were obtained for a set of Dim-8 effective operators sensitive to anomalous cubic and quartic couplings between gauge bosons. The limits obtained featured an interesting complementary with constraints obtained by requiring that the theoretical predictions do not violate unitarity. Many of these results constitute the tightest constraints on such class of models to date. Unfortunately, an attempt to use the measurement results of an observable highly sensitive to CP-odd states ($\mathcal{OO}$) was not as successful as observables sensitive to high-p_T states in constraining anomalous neutral triple gauge coupling parameters. All these results demonstrate clearly that mastering QCD and EWK are both essential for the future of the LHC program and for the advancement of our knowledge.

References

[1] C. Anastasiou, C. Duhr, F. Dulat, F. Herzog, and B. Mistlber, Phys. Rev. Lett. **114** (2015) 212001.
[2] The ATLAS Collaboration, CERN-EP-2023-171, Accepted by EPJC; arXiv:2309.09318 [hep-ex].
[3] S. Camarda et al., Eur. Phys. J. C **80** (2020) 251, [Erratum: Eur.Phys.J.C **80**, (2020) 440]; arXiv: 1910.07049 [hep-ph]. S. Camarda, L. Cieri and G. Ferrera, Phys. Rev. D **104** (2021) L111503; arXiv: 2103.04974 [hep-ph]. [S. Camarda, L. Cieri and G. Ferrera; arXiv: 2303.12781 [hep-ph].
[4] T. Neumann and J. Campbell, Phys. Rev. D **107** (2023) L011506; arXiv: 2207.07056 [hep-ph].
[5] R. Boughezal et al., Phys. Rev. Lett. **116** (2016) 152001; arXiv: 1512.01291 [hep-ph].
[6] The ATLAS Collaboration, Submitted to NPHYS; arXiv:2309.12986 [hep-ex].
[7] J. Haller, A. Hoecker, R. Kogler, K. Mönig and J. Stelzer, PoS ICHEP2022 (2022) 897; arXiv: 2211.07665 [hep-ph].
[8] The ATLAS Collaboration, ATLAS-CONF-2023-004.
[9] H. Georgi and M. Machacek, Nucl. Phys. B 262 (1985) 463.
[10] The CMS Collaboration, Eur. Phys. J. C **81** (2021) 200; arXiv: 2009.01186 [hep-ex].
[11] The ATLAS Collaboration, CERN-EP-2023-221, Submitted to JHEP; arXiv:2312.00420 [hep-ex].
[12] The ATLAS Collaboration, CERN-EP-2023-199, Submitted to PLB; arXiv:2310.04350 [hep-ex].
[13] The ATLAS Collaboration, CERN-EP-2023-199, Accepted by JHEP; arXiv:2310.04350 [hep-ex].